

Reciprocity-based passive monitoring with individual sources

Carlos Almagro Vidal¹, Joost van der Neut¹, and Kees Wapenaar¹

ABSTRACT

Time-lapse changes in the subsurface can be analyzed by comparing seismic reflection data from two different states, one serving as the base survey and the second as the monitor survey. Conventionally, reflection data are acquired by placing active seismic sources at the acquisition surface. Alternatively, these data can be acquired from passive sources in the subsurface, using seismic interferometry (SI). Unfortunately, the reflection responses as retrieved by SI inherit an imprint of the passive-source distribution; therefore, monitoring with SI requires high passive-source repeatability, which is very often not achievable in practice. We have developed an alternative by using active seismic data for the base survey and a single passive source (e.g., a seismic tremor produced by induced seismicity) for the monitor survey. By constraining the source-radiation pattern of the (active) base survey according to the characteristics of the (passive) monitor survey, we succeed in extracting the time-lapse response in the image domain. We tested our method with numerically modeled data.

INTRODUCTION

Study of the earth's subsurface has profited from the use of non-invasive techniques to analyze its structure and to measure the changes occurring in its interior. Techniques related to seismic methods analyze the changes in the mechanical properties of the subsurface. These types of changes can be associated with deformation, fluid flow, temperature variations, or to modifications in material properties (Snieder et al., 2007), and they might be caused by natural (e.g., faulted areas, volcanic zones) or anthropogenic (e.g., gas/oil or water reservoir exploitation) activities. The standard monitoring procedure for analyzing these changes with seismics is the acquisition of

two or more active surveys with controlled sources: one serving as the base and the other(s) as the monitor survey(s) (Greaves and Fulp, 1987; Lumley, 2001).

The challenge of monitoring the changes in the subsurface with passive seismics consists in producing a repeatable analysis by means of naturally occurring sources (Ratdomopurbo and Poupinet, 1995; Snieder and Hagerty, 2004). Seismic interferometry (SI) with coda waves (Snieder, 2006) can make use of these natural or passive seismic sources to monitor the changes in the subsurface that may occur over time (Brennguier et al., 2016). In SI, the crosscorrelation of the recordings from naturally occurring sources between two receiver stations enables the retrieval of the transmission response between these two (Campillo and Paul, 2003). The use of this technique with surface waves from passive sources has enabled the monitoring at volcanic sites (Sens-Schönfelder and Wegler, 2006; Obermann et al., 2013) and producing-reservoir locations (de Ridder and Biondi, 2013).

Additionally, SI can also use the body waves produced by passive sources inside the medium to retrieve the reflection response at the acquisition level (Claerbout, 1968; Wapenaar, 2004). The main condition to apply this technique is to have a sufficiently dense distribution of passive sources in the subsurface. This condition can, for example, be met in reservoir-monitoring applications, in which passive sources are represented by tremors caused by fluid replacement, injection-induced fracturing, or perturbations in the stress patterns in the proximity of the reservoir. This technique enables us to monitor the medium using the retrieved reflection response and study the changes in the subsurface in terms of its reflectivity. The use of an active base survey can be complemented with the resulting virtual-source reflection survey in the role of monitor survey (Ugalde et al., 2011; Boullenger et al., 2014). This approach is referred to as conventional interferometric passive monitoring.

In this monitoring scheme, the retrieval of the reflection response in the monitor state aims to attain the same illumination characteristics as those of the active base survey; however, passive sources are, in most of the cases, sparsely distributed and clustered, thus distorting the illumination of the estimated reflection response and

Manuscript received by the Editor 23 February 2018; revised manuscript received 6 October 2018; published ahead of production 04 December 2018; published online 01 March 2019.

¹Delft University of Technology, Department of Geoscience and Engineering, Faculty of Civil Engineering and Geosciences, 2628 CN Delft, The Netherlands. E-mail: carlos.almagrovidal@gmail.com (corresponding author); j.r.vanderneut@tudelft.nl; c.p.a.wapenaar@tudelft.nl.

© 2019 Society of Exploration Geophysicists. All rights reserved.

leaving an imprint on it. Removing this imprint from the reflection estimate is a nontrivial task and requires illumination balancing for the case of SI by crosscorrelation (Curtis and Halliday, 2010) or solving an inverse problem for other passive SI methods (e.g., Wapenaar et al., 2008; van Groenestijn and Versuur, 2010). Yet, when passive-source illumination is limited to a significantly reduced part of the subsurface, inverse SI methods become severely ill-posed and fail to achieve a good result.

If passive illumination conditions are poor, for instance, in cases in which only a single passive source is available, alternative solutions are required. In this paper, we propose a processing method that adjusts the conditions of the active base survey to those of the passive monitor survey. We design this method by using reciprocity theorems.

Reciprocity-based passive monitoring with individual sources

The correlation function of a single passive source contains correlated events induced by the presence of reflectors in the subsurface. Most of these events represent nonphysical arrivals, except for those trace sections that cover the stationary-phase zone of the reflectors (Snieder, 2004; Wapenaar and Fokkema, 2006; Schuster, 2009). Using correlation functions for time-lapse applications would require the physically unattainable situation of the passive sources to coincide in characteristics and location during the base and monitor

states. By means of seismic reciprocity, however, the effect of a single passive source in one of the states can be replicated as if it had happened at the same location in the other state. This is made possible by formulating the relation between the two states, one represented by the passive source inside the medium and the other by the reflection responses at the acquisition surface. Based on this idea, we propose an alternative monitoring method that requires controlled sources for the base-reflection survey and a single passive source at an arbitrary location for the monitor survey. Because both surveys feature incompatible illumination conditions, this method aims to adjust the conditions of the active base survey to those of the passive monitor survey instead of the other way around, as is the case for already existing methods.

Our monitoring method is based on a two-step approach. The first step aims to adapt the active base survey to the monitor survey by limiting the illumination characteristics, using the information from the passive-source recording. By equalizing the illumination conditions of the base and monitor surveys, we enable the analysis of changes in the subsurface. The second step consists in making use of the physical arrivals among the correlated events in the base and monitor surveys to identify the location of the changes in the medium. We use an adapted depth migration scheme for imaging the correlated events that are related to the monitoring target and in the stationary phase. This migration scheme uses directional constraints based on the illumination characteristics of the passive source (Almagro Vidal et al., 2014), and it is applied identically to the base and monitor surveys. Hence, the artifacts, which could obscure the analysis of changes in the subsurface, are reduced.

We present numerical results of this monitoring scheme in a heterogeneous acoustic medium to which we apply structure and property changes in a reservoir between the base and monitor surveys. In Figure 1, the available data to carry out the time-lapse monitoring are presented. Figure 1a and 1b shows the acquisition and medium characteristics at the base and monitor states, respectively, with coinciding receiver locations (yellow triangles) and different source locations (red stars/red arrow): Multiple active sources are present at the surface during the base survey (Figure 1c), and a single passive source is located during the monitor survey (Figure 1d).

PASSIVE MONITORING

To analyze the changes in the subsurface between the base and the monitor states, we transform the base and monitor surveys such that they share the same illumination characteristics. The modified monitor and base surveys are constructed using either the ballistic or the full fields of the single passive-source recording. The ballistic field corresponds to the part of the wavefield due to direct incidence from the passive source, whereas the full field consists of the complete wavefield including interaction with the free surface.

In this section, we describe for each method the construction of the functions used for the

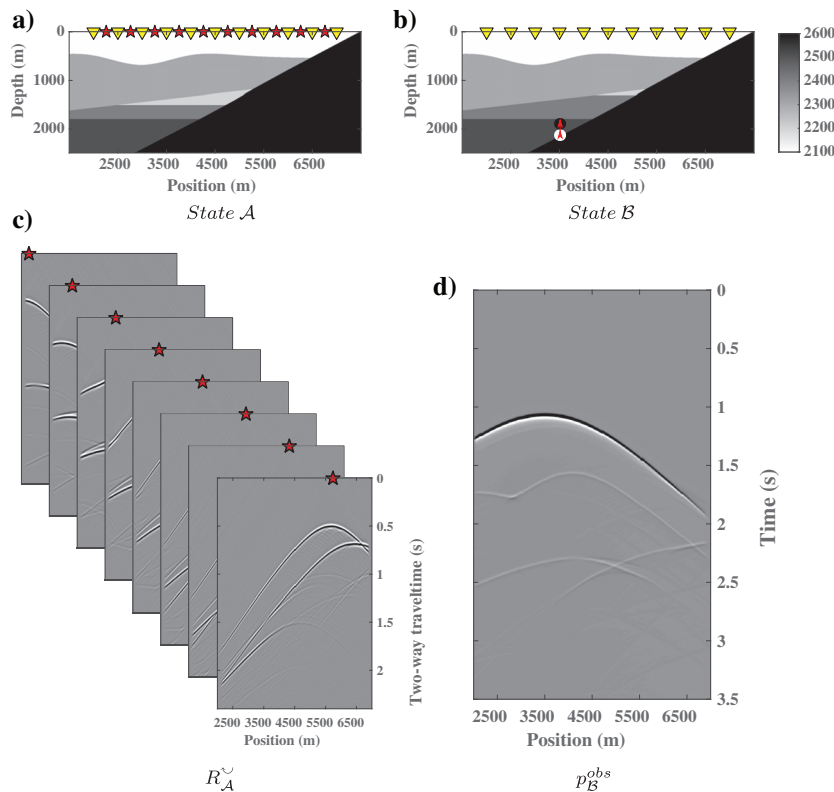


Figure 1. Setup for one of the alternative monitoring schemes: (a) Acoustic velocity model (m/s) at state \mathcal{A} : The controlled sources and receivers are located at the earth's surface (base survey). (b) Model at state \mathcal{B} (monitor survey) with a single passive source (vertical point-force) in the subsurface (symbolized by the red arrow). (c) Reflection-response survey at state \mathcal{A} (R_A^{\vee} , as displayed in (a)). (d) Passive-source recording p_B^{obs} at state \mathcal{B} , as illustrated in (b).

passive monitoring analysis and depict it using the numerical results obtained for a 2D acoustic medium. The changes in the subsurface can be identified in Figure 1, between base state \mathcal{A} and monitor state \mathcal{B} represented in Figure 1a and 1b, respectively. The modeled results use an acquisition array at the free surface with a 5000 m aperture. The receiver sampling is 20 m.

In state \mathcal{A} , we have controlled sources at the receiver locations. To retrieve the reflection response $R_{\mathcal{A}}^{\vee}$ used for the base survey, the source signature is removed and source- and receiver decomposition is applied at the acquisition level to eliminate the corresponding free-surface ghost arrivals. Decomposition results are power-flux normalized (Wapenaar, 1998). In state \mathcal{B} , we use the passive recording $p_{\mathcal{B}}^{\text{obs}}$ of the tremor, which is decomposed at the surface into one-way wavefields and power flux-normalized, but with its unknown source signature preserved. We use for the source of the tremor a vertical point-force source (the red arrow in Figure 1b), but emphasize that the proposed method is independent of the type of passive-source mechanism.

Passive monitoring with the ballistic relation

Our starting point is the following relation between reflection and transmission responses (modified after Wapenaar et al., 2004, equation 22):

$$\begin{aligned} \hat{T}_0^-(\mathbf{x}_A, \mathbf{x}_B, \omega) - \hat{T}^-(\mathbf{x}_A, \mathbf{x}_B, \omega) \\ = \int_{\partial\mathbb{D}_0} \hat{R}^{\vee}(\mathbf{x}_A, \mathbf{x}'_0, \omega) \hat{T}_0^-(\mathbf{x}'_0, \mathbf{x}_B, \omega) d\mathbf{x}'_0, \end{aligned} \quad (1)$$

where $\partial\mathbb{D}_0$ is the acquisition surface, the character $\hat{}$ means that the field is in the space-frequency domain, and ω denotes the angular frequency. In this expression, $\hat{T}^-(\mathbf{x}_A, \mathbf{x}_B, \omega)$ is the upgoing transmission response observed at \mathbf{x}_A , at the acquisition surface, due to the passive source at \mathbf{x}_B in the subsurface, including surface-related and internal multiples. Likewise, $\hat{T}_0^-(\mathbf{x}_A, \mathbf{x}_B, \omega)$ is the equivalent upgoing transmission response acquired at receiver location \mathbf{x}_A but without free-surface interaction. The subscript “0” indicates that the medium is homogeneous above $\partial\mathbb{D}_0$. Regarding the original version of this equation, we have applied source-receiver reciprocity to the transmission responses to describe the wavefields in the left side as upgoing. The term $\hat{R}^{\vee}(\mathbf{x}_A, \mathbf{x}'_0, \omega)$ is the reflection response of the domain below $\partial\mathbb{D}_0$ with free-surface interaction, recorded at receiver \mathbf{x}_A from a source located at \mathbf{x}'_0 on $\partial\mathbb{D}_0$. In the original derivation, all wavefield quantities in equation 1 are power-flux normalized; however, the expression remains valid when the source at \mathbf{x}_B is replaced by an arbitrary type of source (Wapenaar et al., 2011).

Because our passive data correspond to recordings from a real source, the decomposed upgoing fields obtained from the observed wavefield $p_{\mathcal{B}}^{\text{obs}}$ are defined as follows:

$$\hat{p}^-(\mathbf{x}_A, \omega) = \hat{T}^-(\mathbf{x}_A, \mathbf{x}_B, \omega) \hat{s}(\mathbf{x}_B, \omega), \quad (2)$$

$$\hat{p}_0^-(\mathbf{x}_A, \omega) = \hat{T}_0^-(\mathbf{x}_A, \mathbf{x}_B, \omega) \hat{s}(\mathbf{x}_B, \omega), \quad (3)$$

where $\hat{s}(\mathbf{x}_B, \omega)$ is the source signature of the passive source in \mathbf{x}_B . For practical reasons, we approximate $\hat{p}_0^-(\mathbf{x}_A, \omega)$ with the direct-wave estimation $\hat{p}_{\text{dir}}^-(\mathbf{x}_A, \omega)$ of the decomposed upgoing field $\hat{p}^-(\mathbf{x}_A, \omega)$. The error in the direct-wave approximation is due to neglecting the downward-radiating source contribution and internal multiples in the wavefield.

Substituting these wavefields into expression 1 for the monitor state \mathcal{B} yields

$$\begin{aligned} \hat{p}_{\text{dir}}^-(\mathbf{x}_A, \omega) - \hat{p}^-(\mathbf{x}_A, \omega) \\ \approx \int_{\partial\mathbb{D}_0} \hat{R}_{\mathcal{B}}^{\vee}(\mathbf{x}_A, \mathbf{x}'_0, \omega) \hat{p}_{\text{dir}}^-(\mathbf{x}'_0, \omega) d\mathbf{x}'_0, \end{aligned} \quad (4)$$

where $\hat{R}_{\mathcal{B}}^{\vee}$ is the reflection response in the monitor state \mathcal{B} . Applying crosscorrelation on both sides with $\hat{p}_{\text{dir}}^-(\mathbf{x}_0, \omega)$, with \mathbf{x}_0 on $\partial\mathbb{D}_0$, we obtain the normal equation:

$$\begin{aligned} \left(\hat{p}_{\text{dir}}^-(\mathbf{x}_A, \omega) - \hat{p}^-(\mathbf{x}_A, \omega) \right) \{ \hat{p}_{\text{dir}}^-(\mathbf{x}_0, \omega) \}^* \\ \approx \int_{\partial\mathbb{D}_0} \hat{R}_{\mathcal{B}}^{\vee}(\mathbf{x}_A, \mathbf{x}'_0, \omega) \hat{p}_{\text{dir}}^-(\mathbf{x}'_0, \omega) \{ \hat{p}_{\text{dir}}^-(\mathbf{x}_0, \omega) \}^* d\mathbf{x}'_0, \end{aligned} \quad (5)$$

where $\{ \}^*$ stands for the complex conjugation. This expression can be simplified into

$$\hat{C}_{\text{dir},\mathcal{B}}(\mathbf{x}_A, \mathbf{x}_0, \omega) = \int_{\partial\mathbb{D}_0} \hat{R}_{\mathcal{B}}^{\vee}(\mathbf{x}_A, \mathbf{x}'_0, \omega) \hat{\Gamma}_{\text{dir}}(\mathbf{x}'_0, \mathbf{x}_0, \omega) d\mathbf{x}'_0, \quad (6)$$

with the monitor-state correlation function $\hat{C}_{\text{dir},\mathcal{B}}$ defined as

$$\begin{aligned} \hat{C}_{\text{dir},\mathcal{B}}(\mathbf{x}_A, \mathbf{x}_0, \omega) \\ = \left(\hat{p}_{\text{dir}}^-(\mathbf{x}_A, \omega) - \hat{p}^-(\mathbf{x}_A, \omega) \right) \{ \hat{p}_{\text{dir}}^-(\mathbf{x}_0, \omega) \}^*, \end{aligned} \quad (7)$$

and the source function

$$\hat{\Gamma}_{\text{dir}}(\mathbf{x}'_0, \mathbf{x}_0, \omega) = \hat{p}_{\text{dir}}^-(\mathbf{x}'_0, \omega) \{ \hat{p}_{\text{dir}}^-(\mathbf{x}_0, \omega) \}^*. \quad (8)$$

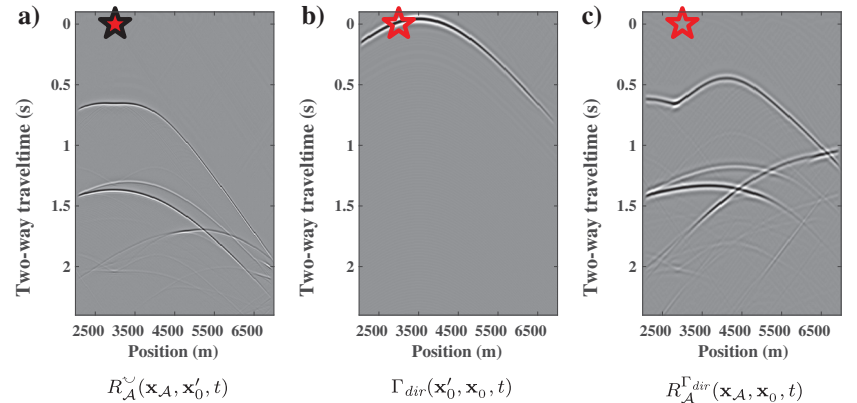


Figure 2. (a) Impulse reflection response $R_{\mathcal{A}}^{\vee}$ at source location $x'_0 = 3000$ m in state \mathcal{A} , with free-surface interaction. (b) Ballistic source function Γ_{dir} at the same location due to the passive-source recording $p_{\mathcal{B}}^{\text{obs}}$ (see Figure 1b and 1d). (c) Illumination-modified reflection function due to the ballistic relation 9 ($R_{\mathcal{A}}^{\text{dir}}$) at virtual source $x_0 = 3000$ m, in the base state \mathcal{A} with the illumination induced from the passive source in the monitor state \mathcal{B} .

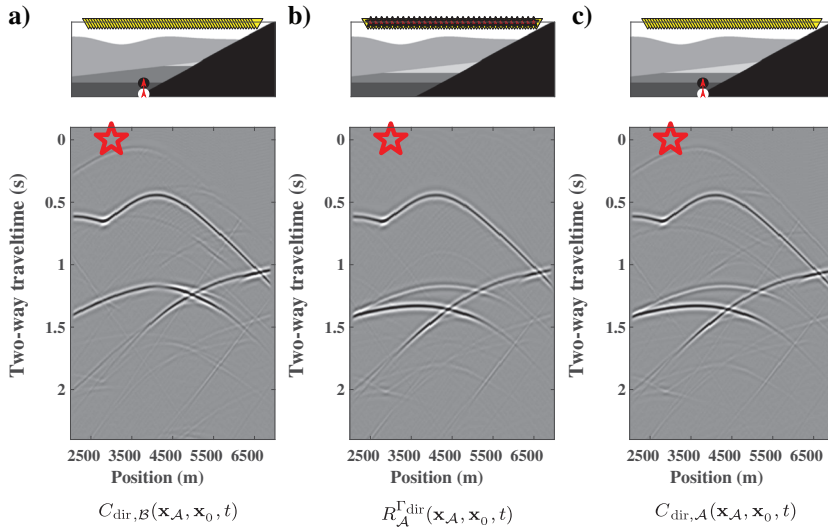


Figure 3. (a) Correlation function of the ballistic relation $C_{\text{dir},B}$ at virtual source $x_0 = 3000$ m, in the monitor state \mathcal{B} . (b) Illumination-modified reflection function of the ballistic relation $R_A^{\Gamma_{\text{dir}}}$ at the same virtual-source location, in the base state \mathcal{A} . This modified reflection function is created with the illumination induced from the passive source in state \mathcal{B} . (c) Correlation function of the ballistic relation $C_{\text{dir},A}$ at the same virtual-source location, in the base state \mathcal{A} .

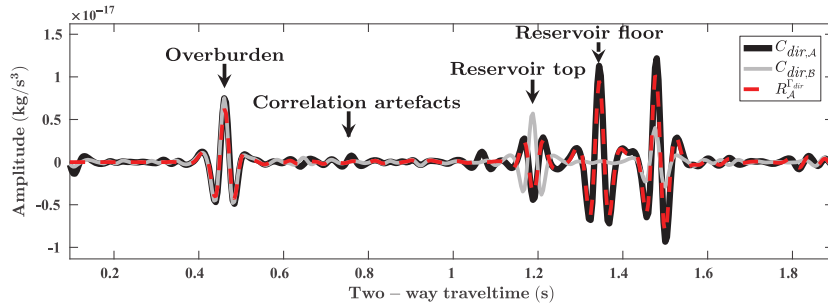


Figure 4. Comparison of correlation functions for the virtual source $x_0 = 3000$ m and receiver $x_A = 4000$ m due to the ballistic relation. The monitor correlation function ($C_{\text{dir},B}$, equation 7, the solid gray line) is to be compared with the illumination-modified base reflection function ($R_A^{\Gamma_{\text{dir}}}$, equation 9, the dashed red line). To corroborate the accuracy of the illumination-modified reflection function of the base, we plot the correlation function of the passive source used in state \mathcal{A} ($C_{\text{dir},A}$, equation 7 for p_A^{obs} , the solid black line).

In representations for interferometry by multidimensional deconvolution, the latter function has also been called the point-spread function (van der Neut, 2013). We call equation 6 the ballistic relation because the reflection response is modified by a source function exclusively composed of the ballistic field of the passive source; hence, equations 7 and 8 are referred to as the monitor correlation function of the ballistic relation and the ballistic source function, respectively.

To compare the base-state reflection response with the monitor correlation function $C_{\text{dir},B}$, we construct the equivalent function for the base state \mathcal{A} by imprinting the illumination characteristics of the passive source onto the corresponding reflection response $R_A^{\Gamma_{\text{dir}}}$, analogous to expression 6. This operation makes use of the same source function $\hat{\Gamma}_{\text{dir}}$:

$$\hat{R}_A^{\Gamma_{\text{dir}}}(\mathbf{x}_A, \mathbf{x}_0, \omega) = \int_{\partial\mathbb{D}_0} \hat{R}_A^{\Gamma_{\text{dir}}}(\mathbf{x}_A, \mathbf{x}'_0, \omega) \hat{\Gamma}_{\text{dir}}(\mathbf{x}'_0, \mathbf{x}_0, \omega) d\mathbf{x}'_0, \quad (9)$$

where $\hat{R}_A^{\Gamma_{\text{dir}}}$ denotes the illumination-modified reflection response of the base state, that is, the equivalent of the correlation function that would have resulted from the passive recording if the same passive source of the monitor state had occurred during the base state. Equation 9 is interpreted in the time domain as a multidimensional convolution of the impulse reflection response $R_A^{\Gamma_{\text{dir}}}$, with the ballistic source function Γ_{dir} . The difference between equations 6 and 9 represents the time-lapse response between the respective reflection responses in states \mathcal{B} and \mathcal{A} according to the illumination-modification introduced by the ballistic source function Γ_{dir} :

$$\begin{aligned} & \hat{C}_{\text{dir},B}(\mathbf{x}_A, \mathbf{x}_0, \omega) - \hat{R}_A^{\Gamma_{\text{dir}}}(\mathbf{x}_A, \mathbf{x}_0, \omega) \\ &= \int_{\partial\mathbb{D}_0} \left(\hat{R}_B^{\Gamma_{\text{dir}}}(\mathbf{x}_A, \mathbf{x}'_0, \omega) - \hat{R}_A^{\Gamma_{\text{dir}}}(\mathbf{x}_A, \mathbf{x}'_0, \omega) \right) \\ & \quad \times \hat{\Gamma}_{\text{dir}}(\mathbf{x}'_0, \mathbf{x}_0, \omega) d\mathbf{x}'_0, \quad (10) \end{aligned}$$

where $R_A^{\Gamma_{\text{dir}}}$ and $C_{\text{dir},B}$ inherit the source-radiation pattern of the same ballistic source function Γ_{dir} and therefore can be directly compared to reveal the time-lapse changes in the reflectivity of the subsurface between states \mathcal{A} and \mathcal{B} according to the illumination angles provided by the passive source. This includes the source characteristics of the passive source in the monitor state. The ballistic source function contains the power spectrum of the passive recording, as does the correlation function $C_{\text{dir},B}$; therefore, for the time-lapse analysis, the source signal is the same in the illumination-modified base reflection function and the monitor correlation function. The direct-wave estimation neglects the internal multiples and causes errors in the base and monitor functions. The monitor correlation function includes correlation artifacts due to the incomplete subtraction in equation 7, and it does not account for other artifacts produced during correlation. Likewise, the source function of the ballistic relation is missing the correlation artifacts caused by the internal multiples; thus, the illumination-modified reflection function of the base state lacks the artifacts necessary for an exact comparison with the monitor correlation function. If internal multiples are high in amplitude, these artifacts can lead to misinterpretations when comparing the correlation functions.

In Figure 2c, we show the illumination-modified reflection function $R_A^{\Gamma_{\text{dir}}}$, obtained from $R_A^{\Gamma_{\text{dir}}}$ (Figure 2a) after its multidimensional convolution with the ballistic source function Γ_{dir} (Figure 2b). During this construction, the information about the subsurface is provided by the impulse reflection response. The ballistic source function imprints the illumination characteristics on the data $R_A^{\Gamma_{\text{dir}}}$, and the result shows the virtually reconstructed correlation function of the tremor in state \mathcal{B} as if it had happened in state \mathcal{A} .

In Figure 3, we show a comparison of the base and monitoring functions using the ballistic relation. Figure 3a displays the correlation function $C_{\text{dir},B}$, which serves as the monitor, and Figure 3b shows the illumination-modified base reflection response $R_A^{\Gamma_{\text{dir}}}$. The

difference of Figure 3a and 3b stems from the changes in the reservoir that we aim to retrieve (the differences between the model in Figure 1a and the model in Figure 1b). Serving as a base reference, Figure 3c shows the correlation function $C_{\text{dir},\mathcal{A}}$, that is, the correlation function of an actual passive source in state \mathcal{A} at the same location as the one in state \mathcal{B} and with the same source spectrum and characteristics. Note the similarities between Figure 3b and 3c, indicating that the radiation patterns of the controlled sources in the base survey have been successfully modified to the illumination characteristics that would be obtained if these data were constructed from the same passive source in the subsurface.

In Figure 4, in which we compare a specific trace from the three panels in Figure 3, the three functions (monitor, base, and base reference) exhibit the same waveform and amplitudes. The overburden remains the same for the base and monitor states, whereas the reservoir top reveals the change of the reservoir properties: The interface remains in the same location, whereas the contrast becomes negative. The corresponding reservoir-floor signal (in this case, this would represent a gas-oil contact), visible in the illumination-modified base reflection function, disappears in the monitor correlation function. Convolution artifacts and amplitude misfits of the reservoir-side and later signals are present because we neglect the internal multiples in the construction of the base $R_{\mathcal{A}}^{\text{dir}}$ and monitor $C_{\text{dir},\mathcal{B}}$ functions, together with the limited aperture of the sources and receivers compared with the depth of the reflectors.

Passive monitoring with the full-field relation

Changes in the subsurface between the two states \mathcal{A} and \mathcal{B} can alternatively be analyzed using the full-field recording of the same passive tremor recording. To this end, we use the following relation between the reflection and transmission responses (modified after Wapenaar et al., 2004, equation 23):

$$\begin{aligned} \hat{T}_0^-(\mathbf{x}_A, \mathbf{x}_B, \omega) - \hat{T}^-(\mathbf{x}_A, \mathbf{x}_B, \omega) \\ = \int_{\partial\mathbb{D}_0} \hat{R}_0^{\sim}(\mathbf{x}_A, \mathbf{x}'_0, \omega) \hat{T}^-(\mathbf{x}'_0, \mathbf{x}_B, \omega) d\mathbf{x}'_0, \end{aligned} \quad (11)$$

where the left side remains the same as in equation 1, whereas the wavefield quantities under the integral now interchange their boundary conditions: \hat{R}_0^{\sim} is the reflection response with the medium homogeneous above $\partial\mathbb{D}_0$, whereas \hat{T}^- is the transmission response including the free-surface interaction. We carry out the corresponding wavefield substitutions from equations 2 and 3 and write the normal equation of relation 11 by applying crosscorrelation of both sides with $\hat{p}^-(\mathbf{x}_0, \omega)$ during the monitor state \mathcal{B} :

$$\begin{aligned} \left(\hat{p}_{\text{dir}}^-(\mathbf{x}_A, \omega) - \hat{p}^-(\mathbf{x}_A, \omega) \right) \{ \hat{p}^-(\mathbf{x}_0, \omega) \}^* \\ \approx \int_{\partial\mathbb{D}_0} \hat{R}_{0,\mathcal{B}}^{\sim}(\mathbf{x}_A, \mathbf{x}'_0, \omega) \hat{p}^-(\mathbf{x}'_0, \omega) \{ \hat{p}^-(\mathbf{x}_0, \omega) \}^* d\mathbf{x}'_0. \end{aligned} \quad (12)$$

The full-field relation can similarly be simplified as

$$\hat{C}_{\mathcal{B}}(\mathbf{x}_A, \mathbf{x}_0, \omega) = \int_{\partial\mathbb{D}_0} \hat{R}_{0,\mathcal{B}}^{\sim}(\mathbf{x}_A, \mathbf{x}'_0, \omega) \hat{\Gamma}(\mathbf{x}'_0, \mathbf{x}_0, \omega) d\mathbf{x}'_0. \quad (13)$$

The full-field correlation function is defined in this case as

$$\hat{C}_{\mathcal{B}}(\mathbf{x}_A, \mathbf{x}_0, \omega) = \left(\hat{p}_{\text{dir}}^-(\mathbf{x}_A, \omega) - \hat{p}^-(\mathbf{x}_A, \omega) \right) \{ \hat{p}^-(\mathbf{x}_0, \omega) \}^*. \quad (14)$$

This function proves to be less sensitive to the approximation of using the direct wavefield when compared to the equivalent expression from the ballistic relation in equation 7. As for the corresponding full-field source function, it turns into

$$\hat{\Gamma}(\mathbf{x}'_0, \mathbf{x}_0, \omega) = \hat{p}^-(\mathbf{x}'_0, \omega) \{ \hat{p}^-(\mathbf{x}_0, \omega) \}^*. \quad (15)$$

This relation becomes a more complicated source function than the one defined in equation 8, but it is easier to construct because no time windowing is involved. Analogous to expression 13, we construct the equivalent function to $C_{\mathcal{B}}$ for the base state \mathcal{A} , by using the base-state reflection response $\hat{R}_{0,\mathcal{A}}^{\sim}$ and the same full-field source function $\hat{\Gamma}$ in equation 15:

$$\hat{R}_{0,\mathcal{A}}^{\Gamma}(\mathbf{x}_A, \mathbf{x}_0, \omega) = \int_{\partial\mathbb{D}_0} \hat{R}_{0,\mathcal{A}}^{\sim}(\mathbf{x}_A, \mathbf{x}'_0, \omega) \hat{\Gamma}(\mathbf{x}'_0, \mathbf{x}_0, \omega) d\mathbf{x}'_0, \quad (16)$$

where $\hat{R}_{0,\mathcal{A}}^{\Gamma}$ represents the full-field relation of the illumination-modified reflection function of the base state. Similar to the monitor correlation function in equation 14, this illumination-modified base reflection function does not rely on direct-wavefield time windowing; therefore, inaccuracies in the time-lapse analysis will exclusively affect the monitor correlation function for the full-field relation. The difference between the base and monitor functions in this case yields a result very similar to expression 10:

$$\begin{aligned} \hat{C}_{\mathcal{B}}(\mathbf{x}_A, \mathbf{x}_0, \omega) - \hat{R}_{0,\mathcal{A}}^{\Gamma}(\mathbf{x}_A, \mathbf{x}_0, \omega) \\ = \int_{\partial\mathbb{D}_0} \left(\hat{R}_{0,\mathcal{B}}^{\sim}(\mathbf{x}_A, \mathbf{x}'_0, \omega) - \hat{R}_{0,\mathcal{A}}^{\sim}(\mathbf{x}_A, \mathbf{x}'_0, \omega) \right) \hat{\Gamma}(\mathbf{x}'_0, \mathbf{x}_0, \omega) d\mathbf{x}'_0. \end{aligned} \quad (17)$$

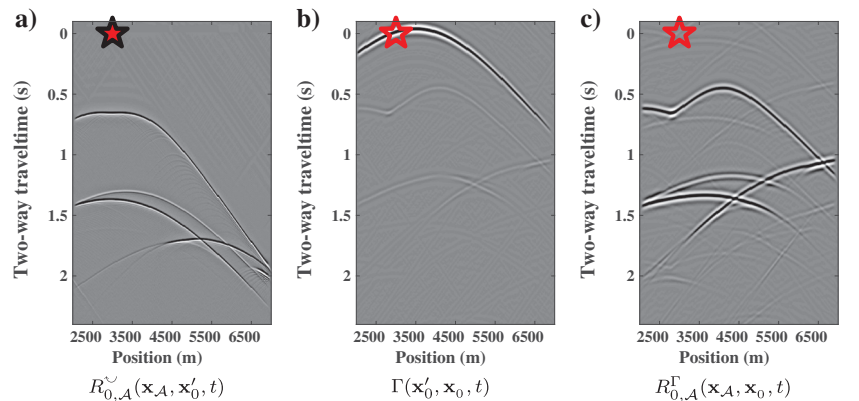


Figure 5. (a) Impulse reflection response $R_{0,\mathcal{A}}^{\sim}$ at source location $x'_0 = 3000$ m in state \mathcal{A} , without free-surface interaction. (b) Full-field source function Γ at the same location due to the passive-source recording p_B^{obs} (see Figure 1b and 1d). (c) Illumination-modified reflection function due to the full-field relation 16 ($R_{0,\mathcal{A}}^{\Gamma}$) at virtual source $x_0 = 3000$ m, in the reference state \mathcal{A} with the illumination induced from the passive source in the monitor state \mathcal{B} .

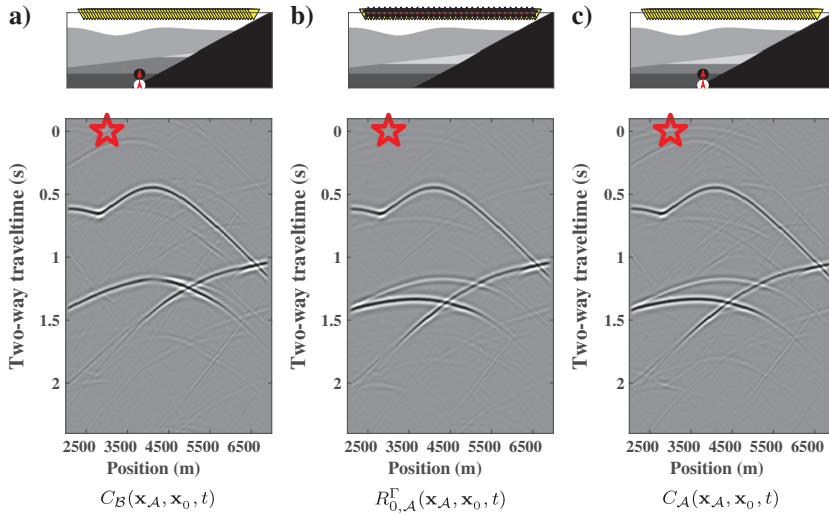


Figure 6. (a) Correlation function of the full-field relation C_B at virtual source $x_0 = 3000$ m, in the monitor state \mathcal{B} . (b) Equivalent illumination-modified reflection function $R_{0,\mathcal{A}}^\Gamma$ at the same virtual-source location, in the base state \mathcal{A} . This modified reflection function is generated with the illumination induced from the passive source in state \mathcal{B} . (c) Correlation function of the full-field relation C_A at the same virtual-source location, in the base state \mathcal{A} .

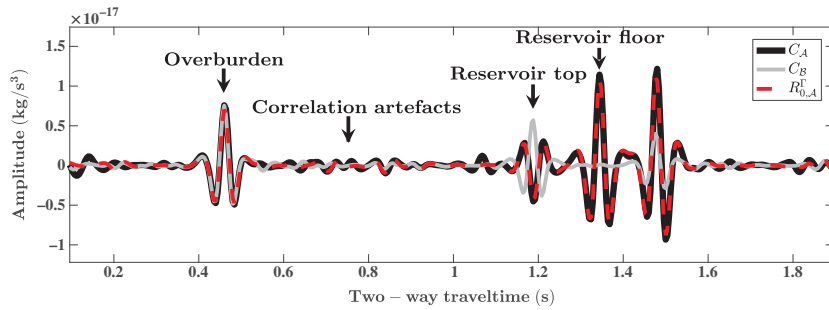


Figure 7. Comparison of correlation functions for virtual source $x_0 = 3000$ m and receiver $x_A = 4000$ m due to the full-field relation. Monitor correlation function (C_B , equation 14, the gray solid line) is to be compared with the illumination-modified reflection function ($R_{0,\mathcal{A}}^\Gamma$, equation 16, the dashed red line). The display of the correlation function of the passive source used in state \mathcal{A} (C_A , equation 14 for p_A^{obs} , the solid black line) confirms the fidelity of the illumination-modified reflection function.

The use of the full-field relation has advantages and drawbacks with respect to the ballistic relation. Correlation and source functions are easier to compute, the illumination-modified reflection function is exact, and the misleading correlation artifacts due to the direct-wave approximation affect only the monitor correlation function. On the other hand, the reflection response data from the base survey require additional processing. The free-surface multiples and source wavelet should be eliminated, either by surface-related multiple elimination (Verschuur et al., 1992) or by estimation of primaries by sparse inversion (van Groenestijn and Verschuur, 2009), providing us the desired impulse reflection response $R_{0,\mathcal{A}}^\vee$ in state \mathcal{A} .

Figure 5c shows the illumination-modified base reflection function $R_{0,\mathcal{A}}^\Gamma$ when carrying out the multidimensional convolution of equation 16 between the impulse reflection response of the base survey $R_{0,\mathcal{A}}^\vee$ (Figure 5a) and the source function Γ (Figure 5b). Once

again, the reflectivity provides the subsurface information of the resulting base function.

In Figure 6, we show the result of the base and monitor functions when using the full-field relation for comparison. Figure 6a shows the monitor correlation function C_B . Figure 6b displays the illumination-modified reflection function $R_{0,\mathcal{A}}^\Gamma$ intended to serve as the base survey. Figure 6c shows the correlation function C_A serving as a reference to the estimated base survey. The features of the virtually created passive-source correlation function resemble the result of the correlation function of the actual passive source in state \mathcal{A} (see the similarities between the results in Figure 6b and 6c).

Figure 7 compares the results of these three functions (monitor, base, and base reference) and shows that the illumination of the passive source is adequately imprinted onto the controlled sources of the base survey. The same waveform and amplitudes are retrieved in the correlation functions. Once again, we identify the same signal changes in the reservoir top and bottom between the base and monitor functions, whereas the overburden signal remains unchanged; however, there is a slightly better matching of the correlation artifacts and the signal of the reservoir flank (see the events at 0.6 – 0.9 s and at 1.5 s, respectively). This confirms that the full-field relation is more reliable than the ballistic one due to its reduced sensitivity to the direct-wave approximation in its formulation, assuming perfect removal of free-surface related multiples in $R_{0,\mathcal{A}}^\vee$.

DIRECTIONALLY CONSTRAINED MIGRATION OF CORRELATION FUNCTIONS

In this section, we aim to use an adapted migration scheme to the illumination-modified base and monitor surveys. This migration scheme was presented in Almagro Vidal et al. (2012) and served to image the correlation functions from

individual passive sources. In this method, the illumination characteristics serve as a directional constraint in the migration process and only those correlated sections that correspond to the stationary phase of primary reflections are imaged. The illumination characteristics are studied by analyzing the source function, which encodes the directional information of the passive-source recording p_B^{obs} at the acquisition array (Almagro Vidal et al., 2014). This analysis identifies the dominant ray parameter \mathbf{p}^{s_0} , which defines the raypath of the specular field of primary reflections from each virtual-source location \mathbf{x}_0 at the acquisition surface $\partial\mathbb{D}_0$.

The migration scheme consists of a forward-extrapolated source wavefield, which uses this directional constraint, and a back-projected receiver wavefield created by either the base or the monitor functions. The forward wavefield is constructed, for a given instant t_0 , using the directional constraint \mathbf{p}^{s_0} as follows:

$$D(\mathbf{x}, \mathbf{x}_0, t_0) \approx \frac{1}{\pi} \Re \int_0^\infty \hat{G}^{\text{GB}}(\mathbf{x}, \mathbf{x}_0, \mathbf{p}^{\mathbf{x}_0}, \omega) \hat{s}(\mathbf{x}_B, \omega) e^{i\omega t_0} d\omega, \quad (18)$$

where $\hat{G}^{\text{GB}}(\mathbf{x}, \mathbf{x}_0, \mathbf{p}^{\mathbf{x}_0}, \omega)$ is a limited asymptotic approximation to the Green's function using a single Gaussian beam with the initial ray parameter $\mathbf{p}^{\mathbf{x}_0}$ at the virtual-source location for any image point \mathbf{x} in the subsurface. The source signal of the passive recording is represented by $\hat{s}(\mathbf{x}_B, \omega)$, which has been extracted from the direct-wavefield arrival. The dominant ray parameter $\mathbf{p}^{\mathbf{x}_0}$ can be estimated from either the ballistic Γ_{dir} or the full-field Γ source functions. Because they should provide a similar result for the dominant ray parameter, the forward wavefield construction in equation 18 remains the same regardless of the function to be imaged, base or monitor and also independently of the reciprocity relation used to build them, ballistic or full field.

For the following explanations of the migration scheme, we focus on the full-field relation. We construct the back-projected field of the illumination-modified reflection function at the base state by adapting the Gaussian-beam summation method described in Popov et al. (2010). First, we correlate the respective illumination-modified reflection function $\hat{R}_{0,A}^\Gamma$ with the individual Green's function approximated with Gaussian beams \hat{G}^{GB} , from every receiver location \mathbf{x}_A , to every image point \mathbf{x} , in multiple directions into the subsurface:

$$\begin{aligned} \hat{R}_{0,A}^{\Gamma, \text{GB}}(\mathbf{x}, \mathbf{x}_0, \mathbf{p}, \omega) &= \{\hat{\Xi}(\mathbf{p}, \omega)\}^* \\ &\times \int_{\partial\mathbb{D}_0} \{\hat{G}^{\text{GB}}(\mathbf{x}, \mathbf{x}_A, \mathbf{p}, \omega)\}^* \hat{R}_{0,A}^\Gamma(\mathbf{x}_A, \mathbf{x}_0, \omega) d\mathbf{x}_A, \end{aligned} \quad (19)$$

where $\hat{\Xi}(\mathbf{p}, \omega)$ stands for a scaling factor for the initial amplitudes of the Gaussian beam as a function of the ray parameter (Popov, 1982). This representation of the base function shows its back projection into the medium in a given direction (expressed in ray parameters \mathbf{p}). Using expression 19, we construct the back-projected field by summing the Gaussian beams over the multiple directions/ray parameters; hence, the back-projected wavefield of the base function, at instant t_0 , becomes

$$\begin{aligned} U_{R_{0,A}^\Gamma}(\mathbf{x}, \mathbf{x}_0, t_0) &= \\ &= \frac{-2}{\pi} \int_{-\infty}^\infty \Re \left\{ \int_0^\infty \hat{R}_{0,A}^{\Gamma, \text{GB}}(\mathbf{x}, \mathbf{x}_0, \mathbf{p}, \omega) e^{i\omega t_0} d\omega \right\} d\mathbf{p}. \end{aligned} \quad (20)$$

As for the back-projected field of the monitor function, we use \hat{C}_B in the same manner:

$$\begin{aligned} U_{C_B}(\mathbf{x}, \mathbf{x}_0, t_0) &= \\ &= \frac{-2}{\pi} \int_{-\infty}^\infty \Re \left\{ \int_0^\infty \hat{C}_B^{\text{GB}}(\mathbf{x}, \mathbf{x}_0, \mathbf{p}, \omega) e^{i\omega t_0} d\omega \right\} d\mathbf{p}. \end{aligned} \quad (21)$$

Because the correlation function C_B and the illumination-modified reflection function $R_{0,A}^\Gamma$ are constructed using the same illumination characteristics, the imaging process uses the same forward wavefield D for each migration result. The imaging condition for the base state correlates D with $U_{R_{0,A}^\Gamma}$

$$I_{R_{0,A}^\Gamma}(\mathbf{x}) = \int_{\partial\mathbb{D}_0} \int_{t_0=0}^T D(\mathbf{x}, \mathbf{x}_0, t_0) U_{R_{0,A}^\Gamma}(\mathbf{x}, \mathbf{x}_0, t_0) dt_0 d\mathbf{x}_0, \quad (22)$$

and equivalently with the back-projected wavefield U_{C_B} for the monitor state

$$I_{C_B}(\mathbf{x}) = \int_{\partial\mathbb{D}_0} \int_{t_0=0}^T D(\mathbf{x}, \mathbf{x}_0, t_0) U_{C_B}(\mathbf{x}, \mathbf{x}_0, t_0) dt_0 d\mathbf{x}_0. \quad (23)$$

Finally, the time-lapse response caused by the changes in the subsurface is portrayed by the difference between the base and monitor imaging results:

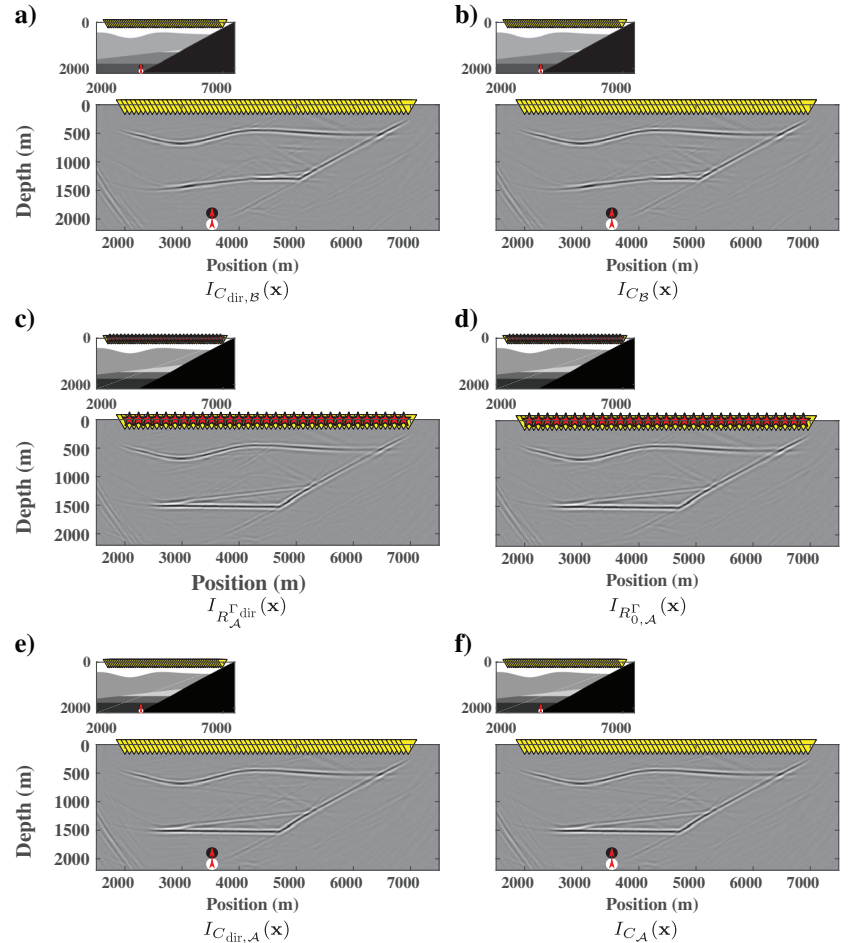


Figure 8. Directionally constrained imaging results of the base and monitor functions using the ballistic and full-field relations. The yellow triangles represent receivers. The red arrow in the subsurface depicts the point-force source used as passive source. (a) Imaging result of the monitor correlation function $I_{C_{\text{dir},B}}$, using the ballistic relation $C_{\text{dir},B}$. (b) Same as in (a) using C_B from the full-field relation. (c) Imaging result of the base function $R_{0,A}^{\Gamma_{\text{dir}}}$, using the ballistic relation. (d) Same as in (c) using $R_{0,A}^\Gamma$ from the full-field relation. (e) Imaging result of the base-state correlation function $C_{\text{dir},A}$ serving as a reference, with the same passive source as in (a), using the ballistic relation. (f) Same as in (e) using C_A from the full-field relation.

$$\Delta I_{B-A}(\mathbf{x}) \propto I_{C_B}(\mathbf{x}) - I_{R_{0,A}^\Gamma}(\mathbf{x}). \quad (24)$$

The same procedure can be applied using the ballistic relation, obtaining $I_{R_{0,A}^{\text{dir}}}$ and $I_{C_{\text{dir},B}}$, using the respective monitor correlation function $C_{\text{dir},B}$ and illumination-modified base reflection function $R_{0,A}^{\text{dir}}$.

In Figure 8, we present the imaging results using the ballistic and full-field relations, migrating all the virtual-source gathers, such as those shown in Figures 3 and 6, respectively. Yellow triangles symbolize receiver locations, red stars are the active sources at the surface, and the red arrow indicates the location and orientation of the passive point-force source. The velocity model used in all migration results is the one from the base state \mathcal{A} (see Figure 1a). Using the full-field relation, Figure 8b displays the migration result I_{C_B} with the reservoir in the monitor state, using the monitor correlation function C_B . The imaging result of the base state $I_{R_{0,A}^\Gamma}$ is shown in Figure 8d.

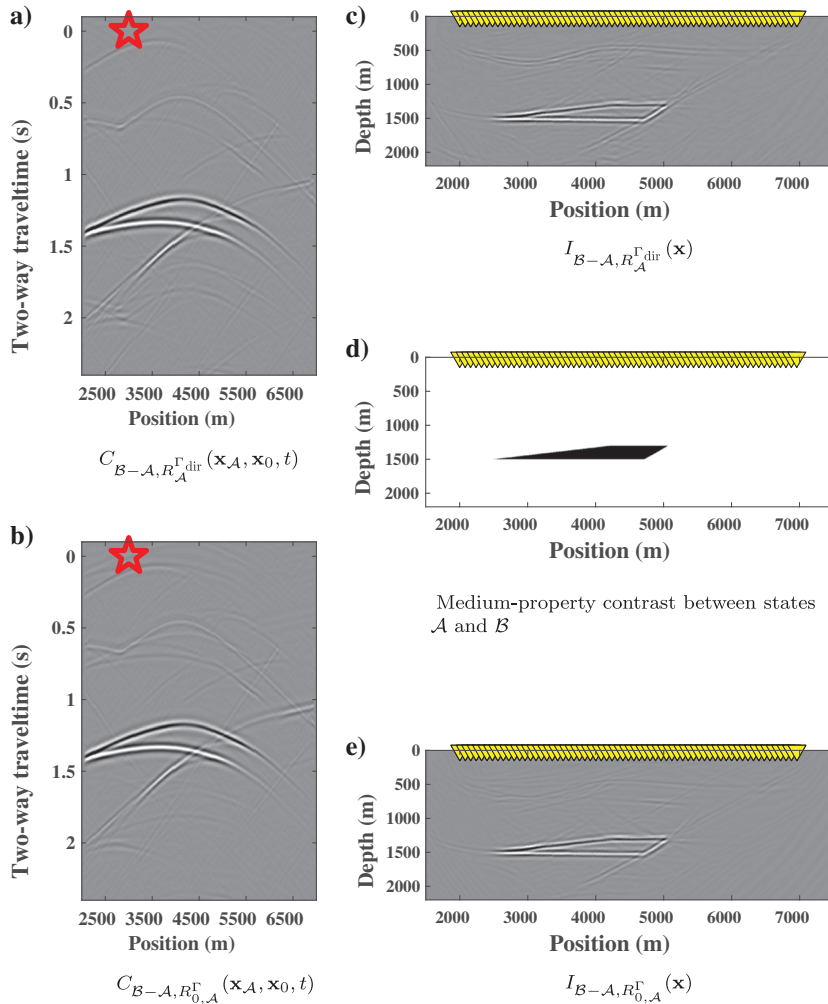


Figure 9. (a) Time-lapse function using the ballistic relation, $C_{B-A, R_{0,A}^{\text{dir}}}$. This is the difference between Figure 3a and 3b. (b) Same as in (a) but using the full-field relation, $C_{B-A, R_{0,A}^\Gamma}$. This is the difference between Figure 6a and 6b. (c) Directionally constrained imaging result of the time-lapse function $C_{B-A, R_{0,A}^{\text{dir}}}$, using the same forward wavefield as for the results in Figure 8. (d) Medium-property contrast between states \mathcal{A} and \mathcal{B} . (e) Same as in (c) but using the full-field relation.

The change in the reservoir contact in the latter with respect to the former is noticeable. These changes are already visible between Figure 6a and 6b. Serving as a reference, Figure 8f shows I_{C_A} , the imaging result using the full-field relation of the correlation function C_A , with an actual passive source in state \mathcal{A} located in the same position as the one in monitor state \mathcal{B} . Figure 8a, 8c, and 8e shows the equivalent results using the ballistic relation. We have thus successfully obtained the time-lapse response in the image domain, using a single passive source only.

The time-lapse response can alternatively be obtained from the left side of either equation 10 or 17. This process avoids the effort of migrating the base and monitor functions. The resulting time-lapse function from equation 17 using the full-field relation reads in this case

$$\begin{aligned} \hat{C}_{B-A, R_{0,A}^\Gamma}(\mathbf{x}_A, \mathbf{x}_0, \omega) \\ = \hat{C}_B(\mathbf{x}_A, \mathbf{x}_0, \omega) - \hat{R}_{0,A}^\Gamma(\mathbf{x}_A, \mathbf{x}_0, \omega). \end{aligned} \quad (25)$$

In a similar manner as discussed before, we construct the back-projected wavefield creating the Gaussian beam representation of the time-lapse function $\hat{C}_{B-A, R_{0,A}^\Gamma}^{\text{GB}}$, as in equation 19, and using the same expression as in equation 20:

$$\begin{aligned} U_{B-A, R_{0,A}^\Gamma}(\mathbf{x}, \mathbf{x}_0, t_0) \\ = \frac{-2}{\pi} \int_{-\infty}^{\infty} \Re \left\{ \int_0^{\infty} \hat{C}_{B-A, R_{0,A}^\Gamma}^{\text{GB}}(\mathbf{x}, \mathbf{x}_0, \mathbf{p}, \omega) e^{i\omega t_0} d\omega \right\} d\mathbf{p}. \end{aligned} \quad (26)$$

Because the time-lapse function is obtained from survey functions with exactly the same illumination characteristics (defined by $\mathbf{p}^{\mathbf{x}_0}$), we use the same forward wavefield described in equation 18, using the same migration velocity model as before, to image the time-lapse response in depth:

$$\begin{aligned} I_{B-A, R_{0,A}^\Gamma}(\mathbf{x}) \\ = \int_{\partial\mathbb{D}_0} \int_{t_0=0}^T D(\mathbf{x}, \mathbf{x}_0, t_0) U_{B-A, R_{0,A}^\Gamma}(\mathbf{x}, \mathbf{x}_0, t_0) dt_0 d\mathbf{x}_0. \end{aligned} \quad (27)$$

Again, this procedure can also be implemented for the corresponding ballistic-relation functions.

Figure 9b shows the time-lapse function $C_{B-A, R_{0,A}^\Gamma}$ for the full-field relation, and Figure 9c displays the imaging result corresponding to the time-lapse response of the medium between states \mathcal{A} and \mathcal{B} , $I_{B-A, R_{0,A}^\Gamma}$. A reference of the time-lapse change of the medium is shown in Figure 9d, in which the contrast is illustrated by subtracting the velocity values of the medium at the base and monitor states (Figure 1a and 1b). Figure 9a and 9c shows the equivalent results using the ballistic relation. These final imaging results are the same as the ones obtained from the subtraction of the imaging results in Figure 8a and 8c, and 8b and 8d, respectively. By applying any of these procedures, the methodology accu-

rately images the time-lapse response of the medium using a single passive source.

DISCUSSION

One condition required for the application of this methodology is the transient behavior of the passive-source signal. This is necessary for the estimation of the direct wave as an approximation to the monitor correlation function (and the source function for the ballistic relation). If the source signal is not sufficiently transient, the signal of the direct arrival might overlap with other arrivals such as the free-surface multiples. This situation is more damaging for the ballistic relation than for the full-field relation. An inadequate removal of the direct arrival will produce additional artifacts in the monitor function. On the other hand, if the removal of the direct wave becomes too extensive, there exists the possibility of removing events critical for the construction of the monitor function.

The quality of the illumination-modified reflection function depends on how well the acquisition surface covers the horizontal location of the passive source. In the numerical examples, we have used a passive source located close to the center of the acquisition array. If the array is too short or the passive source is located horizontally away from it, the result of the multidimensional convolution will produce an incorrect estimation of the illumination-modified reflection function.

This methodology allows, depending on the occurrence of induced seismicity and an adequate receiver-array illumination range, the possibility of intensive monitoring of the reservoir for as many time instances as tremors happen in the subsurface. The time-lapse responses are estimated each time with respect to the active survey. This would suppose the permanent receiver array to be continuously recording over time, but the information obtained would reduce the expense of producing active monitor surveys.

During the imaging process, we used a zero-phase correlation as the imaging condition. The image resolution is thus compromised by the frequency content of the passive-source signal. This feature, however, may be overcome by using alternative imaging conditions (deconvolution techniques, use of extended image conditions) that could partly remove the source signal from the migrated result. Another aspect to exploit is the extension of these techniques to elastic media. This would provide independent imaging results for each combination of wave types.

The use of reflection data for the base survey assumes this has been acquired by active sources. If during the base state, there exists sufficient illumination from passive sources in the subsurface, the base survey can profit from inversion-based passive SI methods to retrieve the impulse reflection response and thus obviate the use of active sources. The advantage of these passive SI methods is that they offer the liberty to retrieve the reflection response either with or without free-surface interaction. This allows the application of ballistic and full-field monitoring methods concurrently, without requiring any source deconvolution and free-surface multiple removal on the base survey; however, this scheme would only hold if all passive sources used in the reflection-response retrieval happen during the same period of time corresponding to the base state, before the changes in the subsurface take place.

CONCLUSION

We have proposed a method that uses a single passive source to image the changes in the reflectivity of the subsurface between two

states. We used the limited illumination from the passive source to impose the same source-radiation characteristics on an active reflection survey. In this process, we reduce the illumination range of the active reflection survey that we use as the base survey, to the limited one provided by the passive-source recording that we intend to use as the monitor survey. We use an illumination-modified reflection function for the base state and a correlation function for the monitor, with exactly the same illumination characteristics. To locate the changes in the subsurface, we propose to apply the migration of the corresponding base and monitor functions, exploiting their limited illumination as a directional constraint. We are thus able to produce the depth-migration results of the base and monitor surveys. These migration results, while using their own respective back-projected receiver wavefields, share the same forward-extrapolated source wavefield. The time-lapse response can alternatively be imaged in depth using the same migration scheme.

In this monitoring scheme, the source mechanism and power spectrum of the passive source are equally imprinted onto the modified base and monitor surveys; therefore, under the conditions of a proper acquisition-array coverage over the passive-source location and a transient behavior of its signal, the source characteristics of the passive source do not hinder the estimation of the time-lapse response.

ACKNOWLEDGMENTS

The authors would like to thank the editor, J. Etgen, A. Malcolm, E. Delaney, F. Broggin, and one anonymous reviewer whose comments contributed to improve the quality of this work. We are grateful to J. Thorbecke for providing the numerical codes that made the results possible (<https://janth.home.xs4all.nl/>).

DATA AND MATERIALS AVAILABILITY

Data associated with this research are available and can be obtained by contacting the corresponding author.

REFERENCES

- Almagro Vidal, C., D. Draganov, J. van der Neut, G. Drijkoningen, and K. Wapenaar, 2014, Retrieval of reflections from ambient noise using illumination diagnosis: *Geophysical Journal International*, **198**, 1572–1584, doi: [10.1093/gji/ggu164](https://doi.org/10.1093/gji/ggu164).
- Almagro Vidal, C., J. van der Neut, D. Draganov, K. Wapenaar, and A. Verdel, 2012, Passive interferometric imaging for limited illumination using slowness diagnosis and directionally constrained Gaussian beam migration: 82nd Annual International Meeting, SEG, Expanded Abstracts, doi: [10.1190/segam2012-1453.1](https://doi.org/10.1190/segam2012-1453.1).
- Boullenger, B., A. Verdel, B. Paap, J. Thorbecke, and D. Draganov, 2014, Studying CO₂ storage with ambient-noise seismic interferometry: A combined numerical feasibility study and field-data example for Ketzin, Germany: *Geophysics*, **80**, no. 1, Q1–Q13, doi: [10.1190/geo2014-0181.1](https://doi.org/10.1190/geo2014-0181.1).
- Brenguier, F., D. Rivet, A. Obermann, N. Nakata, P. Boué, T. Lecocq, M. Campillo, and N. Shapiro, 2016, 4-D noise-based seismology at volcanoes: Ongoing efforts and perspectives: *Journal of Volcanology and Geothermal Research*, **321**, 182–195, doi: [10.1016/j.jvolgeores.2016.04.036](https://doi.org/10.1016/j.jvolgeores.2016.04.036).
- Campillo, M., and A. Paul, 2003, Long-range correlations in the diffuse seismic coda: *Science*, **299**, 547–549, doi: [10.1126/science.1078551](https://doi.org/10.1126/science.1078551).
- Claerbout, J. F., 1968, Synthesis of a layered medium from its acoustic transmission response: *Geophysics*, **33**, 264–269, doi: [10.1190/1.1439927](https://doi.org/10.1190/1.1439927).
- Curtis, A., and D. Halliday, 2010, Directional balancing for seismic and general wavefield interferometry: *Geophysics*, **75**, no. 1, SA1–SA14, doi: [10.1190/1.3298736](https://doi.org/10.1190/1.3298736).
- de Ridder, S., and B. Biondi, 2013, Daily reservoir-scale subsurface monitoring using ambient seismic noise: *Geophysical Research Letters*, **40**, 2969–2974, doi: [10.1002/grl.50594](https://doi.org/10.1002/grl.50594).

- Greaves, R. J., and T. J. Fulp, 1987, Three-dimensional seismic monitoring of an enhanced oil recovery process: *Geophysics*, **52**, 1175–1187, doi: [10.1190/1.1442381](https://doi.org/10.1190/1.1442381).
- Lumley, D. E., 2001, Time-lapse seismic reservoir monitoring: *Geophysics*, **66**, 50–53, doi: [10.1190/1.1444921](https://doi.org/10.1190/1.1444921).
- Obermann, A., T. Planes, E. Larose, and M. Campillo, 2013, Imaging pre-ruptive and co-ruptive structural and mechanical changes of a volcano with ambient seismic noise: *Journal of Geophysical Research: Solid Earth*, **118**, 6285–6294, doi: [10.1002/2013JB010399](https://doi.org/10.1002/2013JB010399).
- Popov, M. M., 1982, A new method of computation of wave fields using Gaussian beams: *Wave Motion*, **4**, 85–97, doi: [10.1016/0165-2125\(82\)90016-6](https://doi.org/10.1016/0165-2125(82)90016-6).
- Popov, M. M., N. M. Semtchenok, P. M. Popov, and A. R. Verdel, 2010, Depth migration by the Gaussian beam summation method: *Geophysics*, **75**, no. 2, S81–S93, doi: [10.1190/1.3361651](https://doi.org/10.1190/1.3361651).
- Ratdomopurbo, A., and G. Poupinet, 1995, Monitoring a temporal change of seismic velocity in a volcano: Application to the 1992 eruption of Mt. Merapi (Indonesia): *Geophysical Research Letters*, **22**, 775–778, doi: [10.1029/95GL00302](https://doi.org/10.1029/95GL00302).
- Schuster, G. T., 2009, *Seismic interferometry*: Cambridge University Press, doi: [10.1017/CBO9780511581557.001](https://doi.org/10.1017/CBO9780511581557.001).
- Sens-Schönfelder, C., and U. Wegler, 2006, Passive image interferometry and seasonal variations of seismic velocities at Merapi Volcano, Indonesia: *Geophysical Research Letters*, **33**, L21302, doi: [10.1029/2006GL027797](https://doi.org/10.1029/2006GL027797).
- Snieder, R., 2004, Extracting the Green's function from the correlation of coda waves: A derivation based on stationary phase: *Physical Review E*, **69**, 046610, doi: [10.1103/PhysRevE.69.046610](https://doi.org/10.1103/PhysRevE.69.046610).
- Snieder, R., 2006, The theory of coda wave interferometry: *Pure and Applied Geophysics*, **163**, 455–473, doi: [10.1007/s00024-005-0026-6](https://doi.org/10.1007/s00024-005-0026-6).
- Snieder, R., and M. Hagerty, 2004, Monitoring change in volcanic interiors using coda wave interferometry: Application to Arenal volcano, Costa Rica: *Geophysical Research Letters*, **31**, L09608, doi: [10.1029/2004GL019670](https://doi.org/10.1029/2004GL019670).
- Snieder, R., S. Hubbard, M. Haney, G. Bawden, P. Hatchell, A. Revil, and D. G. M. W. Group, 2007, Advanced noninvasive geophysical monitoring techniques: *Annual Review of Earth and Planetary Sciences*, **35**, 653–683, doi: [10.1146/annurev.earth.35.092006.145050](https://doi.org/10.1146/annurev.earth.35.092006.145050).
- Ugalde, A., A. Villaseñor, B. Gaité, D. Martí, S. Casquero, and R. Carbonell, 2011, Passive seismic monitoring at an experimental CO₂ geological storage site in Hontomín-Northern Spain: Presented at the 1st EAGE Sustainable Earth Sciences (SES) Conference and Exhibition.
- van der Neut, J., 2013, Downhole interferometric illumination diagnosis and balancing: *Geophysical Prospecting*, **61**, 352–367, doi: [10.1111/j.1365-2478.2012.01122.x](https://doi.org/10.1111/j.1365-2478.2012.01122.x).
- van Groenestijn, G., and D. Verschuur, 2009, Estimating primaries by sparse inversion and application to near-offset data reconstruction: *Geophysics*, **74**, no. 3, A23–A28, doi: [10.1190/1.3111115](https://doi.org/10.1190/1.3111115).
- van Groenestijn, G., and D. Verschuur, 2010, Estimation of primaries by sparse inversion from passive seismic data: *Geophysics*, **75**, no. 4, SA61–SA69, doi: [10.1190/1.3460431](https://doi.org/10.1190/1.3460431).
- Verschuur, D. J., A. Berkhout, and C. Wapenaar, 1992, Adaptive surface-related multiple elimination: *Geophysics*, **57**, 1166–1177, doi: [10.1190/1.1443330](https://doi.org/10.1190/1.1443330).
- Wapenaar, K., 1998, Reciprocity properties of one-way propagators: *Geophysics*, **63**, 1795–1798, doi: [10.1190/1.1444473](https://doi.org/10.1190/1.1444473).
- Wapenaar, K., 2004, Retrieving the elastodynamic Green's function of an arbitrary inhomogeneous medium by cross correlation: *Physical Review Letters*, **93**, 254301, doi: [10.1103/PhysRevLett.93.254301](https://doi.org/10.1103/PhysRevLett.93.254301).
- Wapenaar, K., and J. Fokkema, 2006, Green's function representations for seismic interferometry: *Geophysics*, **71**, no. 4, SI33–SI46, doi: [10.1190/1.2213955](https://doi.org/10.1190/1.2213955).
- Wapenaar, K., J. Thorbecke, and D. Draganov, 2004, Relations between reflection and transmission responses of three-dimensional inhomogeneous media: *Geophysical Journal International*, **156**, 179–194, doi: [10.1111/j.1365-246X.2003.02152.x](https://doi.org/10.1111/j.1365-246X.2003.02152.x).
- Wapenaar, K., J. van der Neut, and E. Ruigrok, 2008, Passive seismic interferometry by multidimensional deconvolution: *Geophysics*, **73**, no. 6, A51–A56, doi: [10.1190/1.2976118](https://doi.org/10.1190/1.2976118).
- Wapenaar, K., J. van der Neut, E. Ruigrok, D. Draganov, J. Hunziker, E. Slob, J. Thorbecke, and R. Snieder, 2011, Seismic interferometry by crosscorrelation and by multidimensional deconvolution: A systematic comparison: *Geophysical Journal International*, **185**, 1335–1364, doi: [10.1111/j.1365-246X.2011.05007.x](https://doi.org/10.1111/j.1365-246X.2011.05007.x).